Journal of
Micro/Nanolithography, MEMS, and MOEMS

SPIEDigitalLibrary.org/jm3

Debris transport analysis at the intermediate focus of an extreme ultraviolet light source

John Sporre
David N. Ruzic

SPIE

Debris transport analysis at the intermediate focus of an extreme ultraviolet light source

John Sporre
David N. Ruzic
University of Illinois at Urbana-Champaign
Department of Nuclear, Plasma, and Radiological Engineering
Center for Plasma Material Interactions
216 Talbot Laboratory, MC-234, 104 South Wright Street
Urbana, Illinois 61801
E-mail: druzic@illinois.edu

Abstract. As extreme ultraviolet light lithography matures, critical deficits in the technology are being resolved. Research has largely focused on solving the debris issue caused by using warm (Te ~ 30 eV) and dense ($n_e \sim 10^{20}$ cm^{-3}) plasma to create 13.5-nm light. This research has been largely focused on the mitigation of the debris between the plasma and the collector optics. The next step of debris mitigation is investigated, namely the effect of debris mitigation on the transport of undesired contaminants to the intermediate focus (IF). In order to investigate emissions from the IF, the Center for Plasma-Material Interactions at the University of Illinois at Urbana-Champaign has developed the Sn intermediate focus flux emission detector. The effects of a secondary RF-plasma, buffer gas flow rate, chamber pressure, and charged plate deflection are investigated. By increasing the chamber pressure to 10 mTorr, flowing 1000 sccm Ar buffer gas, and utilizing charged particle deflection, it is possible to reduce the measured number of post-IF species by greater than 99%. Furthermore, it is shown that typical debris mitigation techniques lead to the development of a plasma near the IF that can be detrimental to post-IF optics. [DOI: 10.1117/1.JMM.11.2.021117]

Subject terms: EUV; intermediate focus; debris mitigation; LDPP; collector optics.

Paper 11101SSP received Jul. 30, 2011; revised manuscript received Nov. 9, 2011; accepted for publication Jan. 16, 2012; published online May 31, 2012.

1 Introduction

The future of extreme ultraviolet (EUV) light lithography hinges upon the ability to surmount the challenges created in using highly energetic, dense (Te ~ 30 eV, $n_e \sim 10^{20}$ cm^{-3}) plasma to create 13.5-nm light.[1–3] One of the biggest issues with switching from the currently used 193-nm deep ultraviolet (DUV) lithography systems to an EUV lithography system is the need to have the entire lithography setup under vacuum. Because 13.5-nm light is readily absorbed at atmospheric gas pressures and by nearly all materials, it is necessary to maintain a low-pressure hydrogen (used for its low absorption of EUV radiation) gas environment, as well as to get rid of the pellicle currently placed between the DUV light source and the collector optics.[4–6] Getting rid of the pellicle consequently requires alternative methods to prevent the energetic ions and neutrals (up to 50 keV) from damaging the collector optics used to focus EUV photons onto the intermediate focus (IF). Such efforts seek to extend the lifetime of the collector optics and reduce the cost of ownership of a tool.[7,8] Typical techniques include the use of collimated foil traps, buffer gas, magnetic field confinement, secondary plasmas of low mass gas species to reduce the coulomb acceleration caused by the rapid expulsion of electrons from the plasma, as well as increasing chamber pressure to increase gas scattering in the short distance between the plasma and the optics.[9–11] While considerable research has been performed in preventing energetic ions and neutrals, as well as condensable Sn plasma fuel from reaching the reflective mirrors, mitigation techniques at the IF have not been widely investigated.

In this paper, several traditional mitigation techniques are investigated with regards to their effect on debris transport to the IF; debris is defined as anything other than EUV photons. In order to analyze the debris emanating from the IF, the Center for Plasma-Material Interactions (CPMI) at the University of Illinois at Urbana-Champaign has developed the Sn intermediate focus flux emission detector (SNIFFED). This device combines a Faraday cup, a residual gas analyzer, a set of microchannel plates with charged particle deflection capabilities, a dual quartz crystal microbalance, as well as a set of witness plates to provide quantitative and qualitative analysis of the undesired flux. For the investigation, CPMI's Xtreme XTS 13-35 EUV light source was modified to include a solid Sn (the current industry standard fuel for creating EUV light) electrode to introduce Sn atoms into a nitrogen Z-pinch plasma using laser ablation. The effects of using an RF-driven secondary plasma, increased buffer gas flow rate, a collimated foil trap, increasing chamber pressure, as well as charged particle deflection, are all investigated with regard to debris transport. It will be shown that by increasing the chamber pressure from 1 mTorr to 10 mTorr, using 1000 sccm Ar buffer gas, a collimated foil trap, and charged particle deflection, it was possible to eliminate greater than 99% of the debris present at the IF without debris mitigation. It will also be shown that despite this reduction in high-energy debris transport, deposition of a non-conductive carbon film persists. This deposition, and debris transport, will be shown to be the result of a secondary plasma created through photoionization or electron impact ionization.

0091-3286/2012/$25.00 © 2012 SPIE

2 Experimental Setup

2.1 *EUV Source, Debris Mitigation, Mock-up Collector Optics*

The EUV light source utilized for the IF debris measurements is a modified Xtreme XTS 13-35 source. The XTS 13-35 source was originally designed to create 35 W of EUV light using a Xe-fueled *Z*-pinch plasma source. In order to provide long-lasting reliable pinch formation, a solid tungsten electrode was used. For these experiments, however, the tungsten electrode was replaced with a Sn electrode to serve as a source of EUV producing atoms. The Xe gas was replaced with N_2 gas to allow for the creation of a dense plasma that does not create EUV light without the introduction of Sn atoms. The N_2 gas was chosen due to its reliable pinch formation, as suggested by the manufacturer. While EUV radiation was created with only the atoms liberated from the electrodes due to the plasma created, an Nd:YAG laser ablation system was installed to create an atomic puff of Sn within the electrode before the *Z*-pinch. In addition to the atomic Sn puff, the existence of which is verified through the use of Si witness plates placed near the electrode in the development of the ablation system, there are also micron-sized droplets formed. For the purpose of this experiment, however, this is not a show-stopper, as the only necessary requirement is the production of EUV light radiation. In reality commercial tools also produce small droplets from laser ablation sources that are of concern to debris transport. The modifications to the XTS 13-35 allow for the production of 2 W of EUV light in 2π sr. using Sn as the EUV emitting fuel. EUV power is measured at the 40 deg angle by an IRD SXUV 20HS/Mo/Si photodiode (12.2 to 15.8 nm band measurement), which is coupled with a one-bounce reflection off of a Mo/Si 50 multi-layer mirror to measure EUV light production. The EUV power measurement is independent of the angle, for the most part due to isotropic light emission.

The Nd:YAG laser is operated at 100 Hz with 125 mJ per pulse at 532-nm harmonic. The beam is reflected off of four mirrors and focused down to a 1-mm spot on the Sn electrode through a quartz window; the resulting beam fluence at the electrode is 9.6 ± 1.6 J/pulse-cm^2 and an average power of 960 ± 160 W. The beam pulse lasts approximately 10 ns, as reported by the manufacturer. Synchronization between the laser and the EUV source is performed by triggering the discharge of the *Z*-pinch capacitors at the start of the laser pulse. This results in the ablated plume of Sn being located inside of the anode cavity during the moment of EUV plasma formation.

Attached to the XTS 13-35 source is the Xtreme Commercial EUV Emission Diagnostic (XCEED) chamber as shown in Fig. 1. The XCEED chamber enables the placement of the mock-up collector optics, as well as provides access for SNIFFED at the IF. Two turbo pumps and a rough pump are attached to the chamber to achieve a base pressure of 1×10^{-6} Torr. A variable gate valve between the chamber and one of the gate valves allow for increases in pressure up to 20 mTorr with full gas flow. The N_2 pinch gas is introduced with a flow rate of 100 sccm, achieving an operating pressure of 0.7×10^{-3} Torr. The Ar buffer gas is introduced near the pinch with flow rates up to 1000 sccm. This is the minimum operating pressure that can be utilized with the XTS 13-35; further reduction in pressure does not allow for the ignition of a plasma.

In order to investigate the debris transport to the IF, a two-shell mock-up collector optic was installed between the plasma and the simulated IF, with the line-of-sight trajectory being blocked by the support structure. The two shells are 12.7 and 43.2 cm in diameter to provide specular reflection at 10 deg and 30 deg from the normal line of the *Z*-pinch cathode. The optic is constructed out of stainless steel sheets, which do not provide complete reflection of EUV light but do allow an investigation into the reflection of debris off the collectors. A mock-up was utilized as a replacement to an industry grazing incidence collector due to the extravagant expense of such a device. Reflections can still be investigated with a stainless steel surface, and as such it is not necessary to implement the multilayer surfaces implemented in true EUV lithography sources. Debris mitigation is implemented using several methods. The first method, a collimated foil trap, is located between the pinch and the collector optics. When coupled with Ar buffer gas, this device serves to deflect energetic ions and neutrals into the tungsten foils aligned radial to the plasma. A one-turn RF antenna coil is also used to create a 100 W secondary plasma between the plasma and collimated foil trap. The created plasma reduces the pull of rapidly ejected EUV plasma electrons on ions, thus reducing the ion energies observed at the collector optic.

2.2 *Sn Intermediate Focus Flux Emission Detector (SNIFFED)*

The SNIFFED apparatus, diagrammed in Fig. 2, consists of five different diagnostics placed 25 cm from the IF to analyze debris from the 10 deg specular reflection angle. The first diagnostic is a shielded Faraday cup used to measure the charge of any charge flux. The outer shield is electrically isolated from the interior cup, to allow charge discrimination between ions and electrons, with a 1-mm orifice for charge flux measurements. The interior cup current is measured using the oscilloscope across a 50-ohm resistor. The second diagnostic, a dual quartz crystal microbalance, serves to measure any ongoing erosion or deposition during the operation of the EUV source. One of the crystals is covered for the duration of the measurement process, and its signal is subtracted from the other crystal's signal to negate any temperature effects providing false conclusions. This detector provides an indication of any possible damage to down line optics. The third diagnostic in SNIFFED is a residual gas analyzer, which provides an analysis of what gas species are transmitted through the IF. The RGA is capable of measuring up to 100 amu species, high enough to measure molecular compounds and any atomic species used in the EUV source chamber. This detector also allows for detection of hydrocarbon contaminants from pumps and chamber contamination. The fourth diagnostic is a set of dual micro-channel plates equipped with two charged plates for charged particle deflection. These dual micro-channel plates, when biased at -2500 V, create a measurable electron signal when impacted by energetic ions or neutrals greater than 100 eV. The charged particle deflector plates allow for the analysis of the charged versus neutral energetic flux and combine to allow for the detection of any energetic species that might cause energetic impact damage to down line

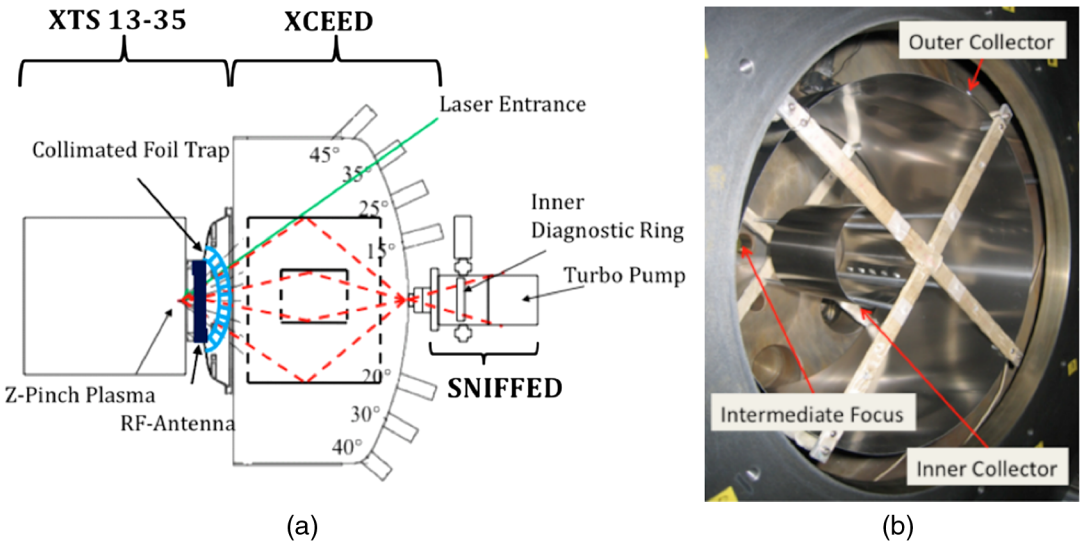

Fig. 1 The experimental apparatus consists of the XTS 13-35 EUV source coupled with the Xtreme Commercial EUV Emission Diagnostic (XCEED). The XCEED chamber holds the mock-up collector optic, which specularly reflects light to the Sn intermediate focus flux emission detector (SNIFFED).

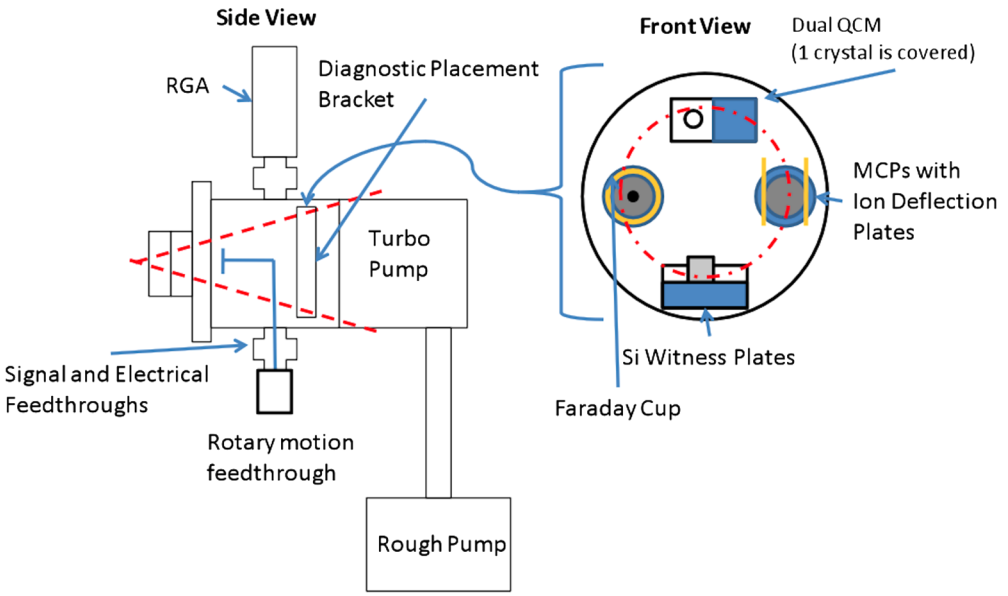

Fig. 2 The SNIFFED chamber consists of five diagnostics: a dual quartz crystal microbalance, silicon witness plates, microchannel plates with charged particle deflection, a Faraday cup, as well as a residual gas analyzer. These diagnostics are placed on the annulus that corresponds to 10 deg specularly reflected light.

optics. Based on time-of-flight analysis, the microchannel plates also allow for a determination of the timing between plasma formation and flux arrival time. In order to prevent arcing between the plates, the SNIFFED chamber is maintained at 5×10^{-7} Torr. When coupled with the Faraday cup, it is possible to know a relative flux measurement of ions. The last diagnostic is a set of Si witness plates placed both in and out of line of sight to the IF point. Each Si witness plate is masked to provide pre- and post-exposure analysis using a scanning electron microscope. When coupled with the quartz crystal microbalance, it is possible to investigate the effect of an erosive or depositional flux emanating from the IF. All told, these five different diagnostics provide the ability to quantitatively measure the charge, quantity, arrival time, residual presence, and detrimental impact of any debris flux being transported to the IF by debris mitigation techniques and the collector optics.

3 Experimental Procedure

The experiments performed are listed in Table 1. As mentioned previously, there are five different mitigation methods utilized: a collimated foil trap, buffer gas, a variation in pressure, secondary plasma, and *E*-field diversion. For each experiment, the XTS 13-35 modified EUV source is pulsed at 20 Hz. Buffer gas flow rates are set on the mass flow controller and the gas is allowed to flow until stabilized within

Table 1 Shown are the experimental settings used to analyze the mitigation schemes' effect on debris transport to the IF.

Trial number	Nitrogen flow rate (sccm)	Ar flow rate (sccm)	RF On/Off
1	100	0 (1 mTorr)	Off
2	100	500 (1.75 mTorr)	On
3	100	1000 (2.25 mTorr)	On
4	100	200 (1.25 mTorr)	Off
5	100	500 (1.75 mTorr)	Off
6	100	1000 (2.25 mTorr)	Off
7	100	1000 (20 mTorr)	Off
8	100	1000 (10 mTorr)	Off

the chamber. The quartz crystal micro-balances are turned on at the beginning of the data acquisition to monitor the addition or removal of mass from the crystals and turned off between parameter changes. With the pinch and the laser running, the Faraday cup signal is observed with the starting time on the oscilloscope corresponding to the discharge of the capacitors. The signal is measured using a running 100-pulse average to overcome oscillating variations from pulse to pulse. The Faraday cup signal was observed for signals throughout the time between pinches to observe any possible latent charge buildup. For the micro-channel plate measurements, the oscilloscope was set for 500 us/div and 50 mV/div to observe the incident flux measurement signal. A histogram function was utilized to tally the total measured particle hits observed over a one-minute period. The charge deflecting plates create a 3000 V potential across a 3-cm gap to divert ions before they reach the micro-channel plates.

It was quickly observed through the first two trials that adding the secondary RF plasma did not help to mitigate the debris, rather it added to the total flux over a longer period of time. Consequently, these measurements were ceased after the third trial. The RF-plasma could not be ignited with only 200 sccm flow rate. The additional pressures, as listed on trials 6 to 7, show that the chamber's pumping capabilities were intentionally reduced to increase the pressure within the chamber. At 1000 sccm Ar buffer gas flow rate, the one Osaka turbo is not adequate in removing all of the additional gas being introduced. By installing two turbomolecular pumps on the XCEED chamber and installing a gate valve on one of them, it was possible to partially close the gate valve to create a more stable pressure. The intent of this increase in pressure is to reduce the mean free path of an atom within the chamber.

4 Results and Discussion

In a Sn-fueled EUV source, there are four predominant sources of debris transported to the IF: energetic plasma species that are reflected off of the collector optics and focused onto the IF; energetic plasma species that are scattered off of buffer gas atoms within the chamber; Sn that is deposited on the collector optics and consequently sputtered off; and contamination from the walls of the chamber. The following experimental analyses investigate the effect of debris mitigation methods on the transport of this debris to the IF. It should be noted that the experiments were performed in a random order to prevent artificial trends being observed due to time variation of the EUV source and collector optics. Such variations would be caused by the observed Sn deposition on the mock-up collector optic, as well as surface heating of the chamber and consequent desorption of contaminants. Due to the random nature of the testing, however, these are not evident trends in the resulting data.

The first investigation involves the use of the residual gas analyzer attached to SNIFFED. As mentioned previously, this detector is used to analyze the presence of gas line contamination. There is only one main observation derived from this analysis, however, which is that the partial pressures of the argon buffer gas and nitrogen fuel gas increase with an increase in buffer gas flow rate. This was a consequence of the fact that as the rate of buffer gas injection is increased, the pressure within the EUV source chamber is increased. Water vapor (from an inadequate chamber bake-out) and hydrocarbons (namely from rough pump oil allowed to deposit onto the chamber walls during venting) were present, but not in large enough quantities to be of concern.

The quartz crystal microbalance measurements shown in Fig. 3 reveal the occurrence of deposition at the IF. The possible deposited species are Sn atoms from the electrode, nitride films from the cracking of the nitrogen fuel gas, oxides from ionized and cracked water vapor molecules present in the chamber, or carbon contamination present on the chamber wall. The leading suspect appears to be carbon contamination, however, as will be shown in the Si witness plate analysis. Figure 3(a) shows the deposition rate as a function of increasing chamber pressure. It is observed that after the first increase from 1 to 1.25 mTorr, the deposition rate is decreased by a factor of 5. However, an additional increase in pressure does not serve to further alleviate deposition on the crystal surface. Figure 3(b) shows the deposition rate as a function of buffer gas flow rate. It is clear from this figure that the initial injection of 200-sccm Ar buffer gas has more effect than increasing chamber pressure. The deposition rate with further increase in buffer gas is largely unaffected, and stands to reason that most of the depositing debris is mitigated by the first 200 sccm.

Adding buffer gas between the EUV plasma and the collimated foil trap increases the number of collisions that the energetic ions and neutrals experience as they enter the chamber. The scattering collisions deflect these energetic species into the tungsten foils where they can deposit most of their energy. This has the effect of reducing the energy of the species reaching the collector optic, and as such there will be less sputtering of downstream surfaces. This includes a reduction in the sputtering of hydrocarbons off of the walls, which likely explains the immediate reduction in the deposition rate observed at the IF. Additional increases in buffer gas flow rate are evidently inconsequential in increasing the pressure between the foil trap and the source, and do not further reduce the observed deposition rates caused by energetic species reaching the collector optics. The lack of deposition rate change with increasing pressure suggests that the observed deposition rates beyond 200 sccm

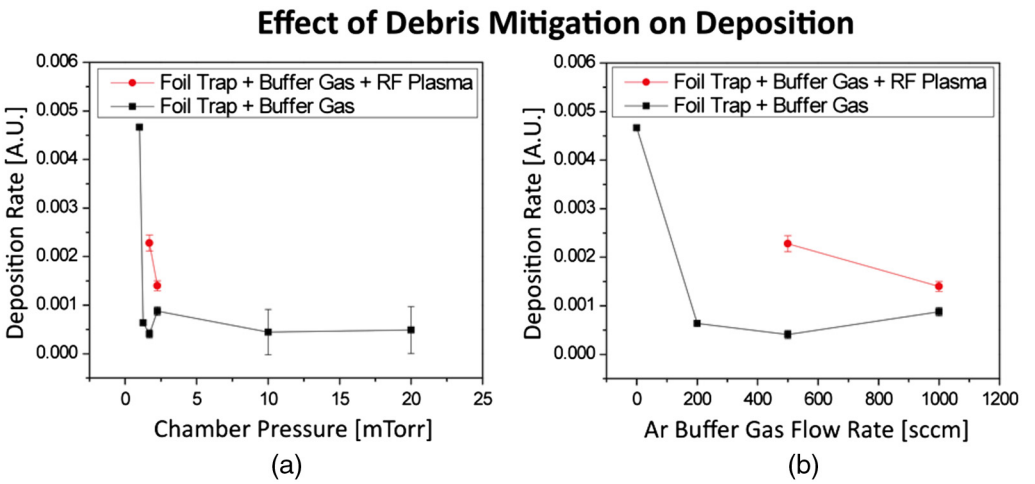

Fig. 3 The increase in flow rate of Ar buffer gas beyond 200 sccm drastically reduces the amount of deposition occurring at the IF. The RF secondary plasma leads to additional deposition. These measurements were performed with the source operating at 20 Hz, 100 sccm N_2.

are a consequence of either photon-hydrocarbon cracking or the presence of a persistent-induced plasma liberating contaminants from the chamber surface. The use of the secondary RF plasma serves only to increase the number of ionized species and consequently increases the deposition rate.

The Faraday cup measurements shown in Fig. 4 reveal that throughout the period between EUV plasma pinches there exists a positive flux reaching the IF. The non-zero current of low pressure (<10 mTorr) measurements suggests the presence of sustained ionization. This current production is driven by secondary ionization from the initial *Z*-pinch plasma expansion, as well as delayed non-EUV photoionization at the back-end of the discharge. Native gas species, sputtered neutrals, as well as residual *Z*-pinch species all contribute to the ionized species being observed. More interesting, however, is when 1000 sccm Ar is injected with an additional increase in chamber pressure to 10 mTorr. At this pressure, chamber-wide plasma is created before EUV formation. This process suggests that at 10 mTorr a critical pressure is reached at which point a sustained plasma can exist. This is allowed by the increased interaction between electrons and neutrals with the reduction in mean free path. The plasma then diffuses to the walls and is largely extinguished (besides the background charged flux) within the first 1 ms after EUV formation. If one assumes that all species are singly ionized during this period, a flux of $1.0 \pm 0.15 \times 10^{11}$ ions/cm^2 is observed. This flux increases to $1.38 \pm 0.18 \times 10^{11}$ with an increase in pressure to 20 mTorr as shown in Fig. 5.

The initial spike in ion flux found in both traces is a consequence of the photoionization of the Faraday cup surface from the reflected photons with energy greater than 7.7 eV (the photoionization energy threshold of copper). The EUV source, in addition to creating ~100 eV EUV photons, also generates deep ultraviolet photons with wavelength less than the ~160 nm required to photo-ionize copper. These photons are created during the pinching of the plasma. The discharging of the capacitors, and consequent recharging, presents

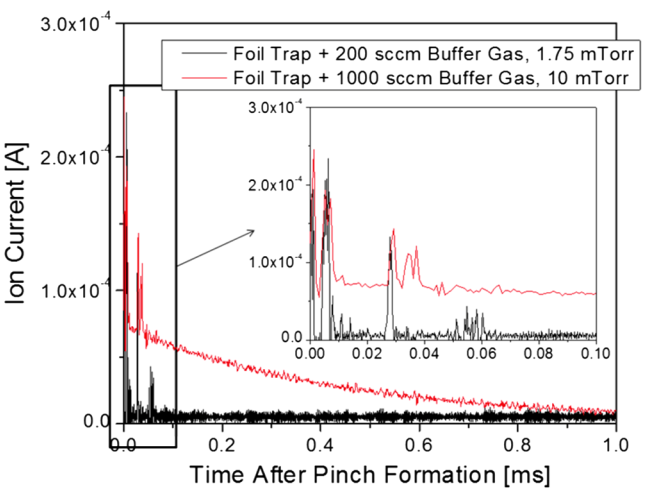

Fig. 4 Diffuse low energy plasma is observed to be created by photo or electron ionization in the moments precluding EUV light formation. The plasma then diffuses, but there is a noticeable positive flux throughout the duration between pinches.

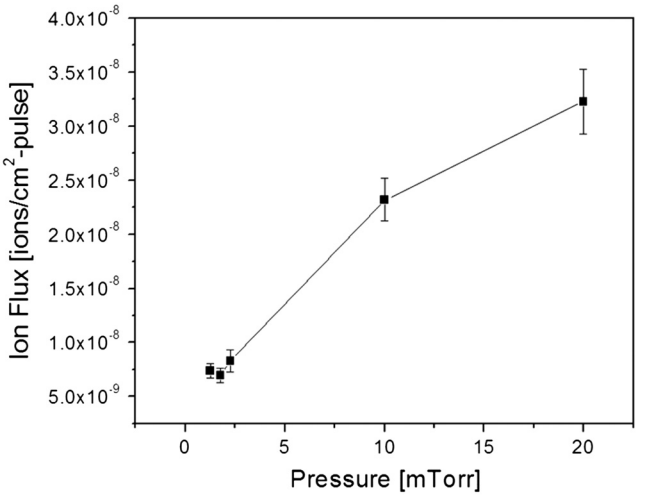

Fig. 5 A baseline ion flux of ~3×10^{10} ions/cm^2 is observed at low pressures through the first 1 ms after the discharging of the capacitor banks. Increasing the pressure above 10 mTorr results in the ignition of a secondary plasma that diffuses to the chamber walls in the first millisecond.

as electromagnetic noise over the first 5 μs and 30 to 40 μs following the formation of EUV respectively; there is also a noise peak at 60 μs that is attributable to the capacitor bank charging. Unfortunately, due to the random nature of its occurrence, this peak is not removable with a background measurement. The observed charged flux prior to 3 μs, however, provides conclusive evidence for the occurrence of an induced non-pinch plasma formation. The arrival time of the energetic ions/neutrals from the Z-pinch plasma take more than 5 μs to arrive at the chamber wall in direct line of sight. Because the positive flux is observed before 3 μs, it is a direct consequence of either electron-neutral ionization from the electrons leaving the Z-pinch plasma, or from photoionization of neutrals in the chamber.

While the Faraday cup provides a quantitative analysis of the charge state of all charged debris incident on the IF, the microchannel plates provide a way to relatively quantify the effects of debris mitigation on charged and neutral high energy (>100 eV) species. The effects of each debris mitigation technique on flux are outlined in Fig. 6, with the total number of hits on the detector being summed over a 4.7 ms period after EUV formation. The initial usage of the foil trap with 500 and 1000 sccm in conjunction with the secondary RF plasma reveals that the mitigating effects of buffer gas are negated by the transport of more energetic neutral species with the use of the secondary plasma (ion diverter plates yielded no difference in flux measurements). Of more interest, however, is the fact that increasing buffer gas from 0 to 200 sccm (now no longer using the secondary RF plasma) decreased the high-energy neutral flux by 97%. This is also in accordance with the deposition observations that showed a drastic decrease with an introduction of only 200 sccm. Increasing flow rate to 500 sccm further reduces the

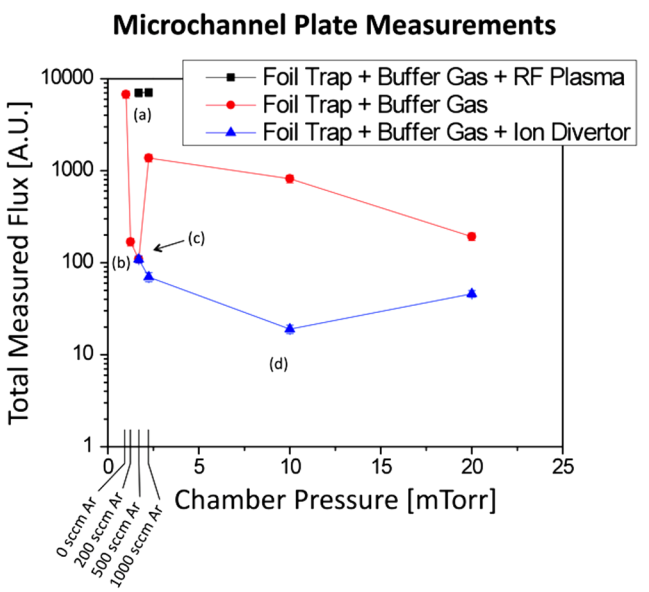

Fig. 6 Starting at (a), it is observed that the secondary RF plasma does not reduce the amount of debris impingent on the IF. Discontinuing the use of the RF plasma, and increasing buffer gas flow rate (b) reduces the flux until 1000 sccm is reached. At this point (c) the total flux increases, and the flux becomes primarily ions. Increasing the pressure (d) reduces this flux with the optimum reduction in flux observed at 10 mTorr. These measurements are summed over the first 5 ms after the EUV plasma formation.

observed debris, but at 1000 sccm, the total (neutral and ion) flux increases by 1100%. At this flow rate, however, it is observed that the total flux is no longer solely neutral; in fact the flux is 95% high energy ions. As pressure is increased, the ion flux and neutral flux is decreased. With the use of ion diversion through the application of an electric field, the optimized debris mitigation case was observed to be the 10 mTorr trial. Using the foil trap, with 1000 sccm Ar buffer gas, and electric field diversion, it was possible to remove 99.7% of the unmitigated flux observed at the IF. It should be noted that the lack of charged flux in the lower flow rate cases does not necessarily mean there is no charged flux reaching the IF. As was shown in the Faraday cup measurements, there is charged flux in reaching this location. The reason this charged flux is not observable by the microchannel plates is because it is not energetic enough to be measured. These results clearly show that the energetic species measured with the microchannel plates originate from the EUV plasma, while the diffuse plasma observed with the Faraday cups originates as a bi-product of the EUV plasma.

Observing the measured flux on a case-by-case basis for the 500 sccm, 1000 sccm, and consequential pressure increases to 10 and 20 mTorr, reveals an interesting phenomenon. As evidenced in Fig. 6, the increase from 500 sccm [Fig. 7(a)] to 1000 sccm [Fig. 7(b)] drastically increases the observed total flux at the IF. Consequent reductions in flux are also observed with an increase of pressure from 2.25 mTorr to 10 mTorr Fig. 7(c) and 20 mTorr Fig. 7(d). Of interest, however, is the fact that these increases in pressure delay the time of arrival of the peak of flux. At 2.25 mTorr, this peak occurs at approximately 0.8 ms after EUV formation, while at 10 mTorr this peak occurs at nearly 3.8 ms. This peak is not evident at 20 mTorr, which will be explained shortly, but appears to begin to form at the end of the data acquisition period. Unfortunately oscilloscope limitations prevented measurement of periods longer than 5 ms with appropriate data resolution. The delay in peak arrival time with increasing pressure can be explained by considering the collisions that a Z-pinch accelerated atom (the only species with enough energy to be measured by the microchannel plates) undergoes before reaching the IF. The mean free path of an atom is directly proportional to pressure, and consequent increases in pressure will result in a linear increase in the number of collisions between an energetic ion and the background gas. This is observed in the 3 ms shift in peak arrival time between 2.25 mTorr and 10 mTorr. The ratio of arrival time is ~4.4, which corresponds to the 4.4 factor increase in pressure. A similar increase in the arrival time factor of ~1.3 is observed in transition from 1.75 mTorr to 2.25 mTorr. As such, it would be logical to conclude that the arrival time of the peak of energetic debris for the 20 mTorr case would occur at ~7.6 ms after pinch formation, thus its lack of existence on these plots. These results clearly show that the arrival of energetic Z-pinch formed species at the IF is a function of chamber pressure.

The influence of gas scattering on the arrival time of energetic species at the IF suggests two different possibilities for the persistence of energetic ions. The mean free path of an ion travelling through a 1 mTorr Ar filled chamber is ~0.3 m, while the mean free path for a 20 mTorr chamber

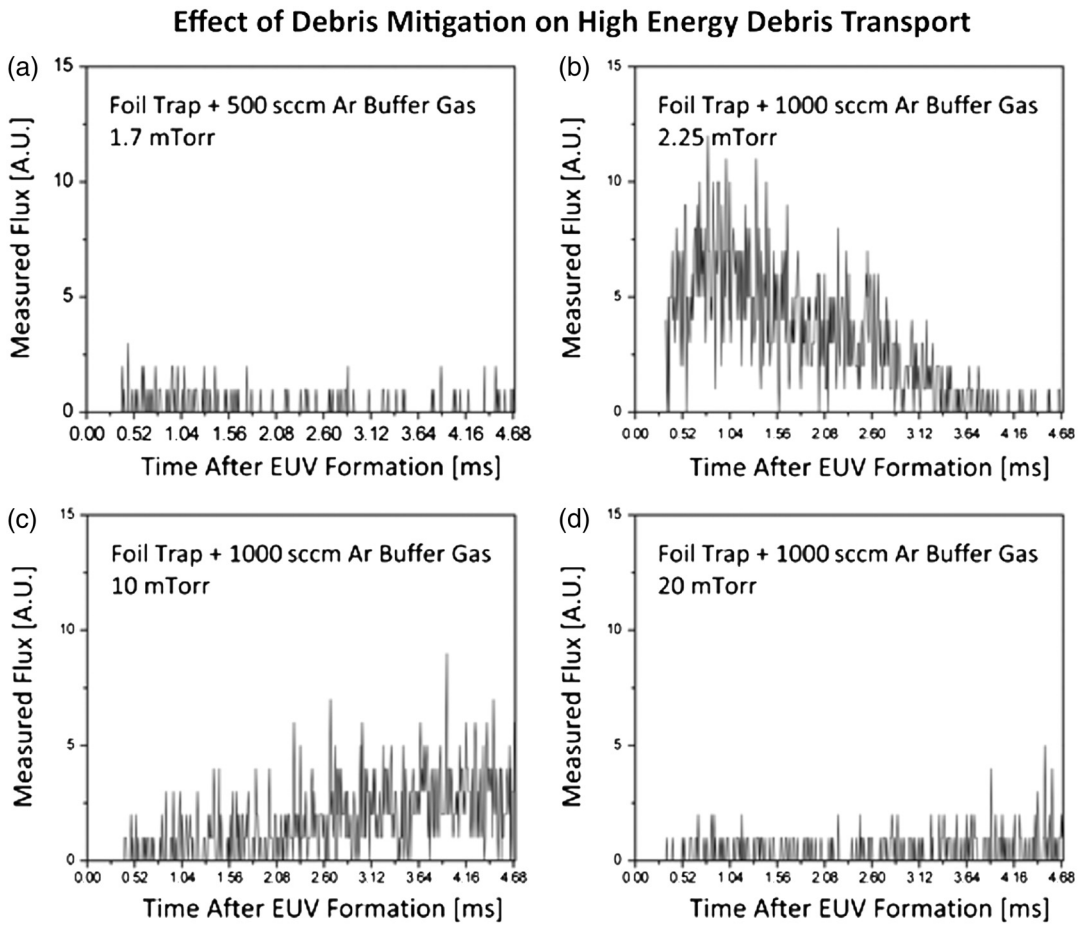

Fig. 7 An observation of the microchannel plate hit counts, summed over a one-minute period, reveals that the addition of pressure to the chamber serves to increase the delay in arrival time of high-energy ions.

is only ~2 cm. At low pressures, it is far more likely for an energetic ion to have neutralizing wall collisions before it reaches the IF. Furthermore, it was observed with the Faraday cup that there is no residual decaying plasma at these low pressures. At 20 mTorr, however, there are a greater number of collisions and a higher likelihood that a wall will not neutralize the energetic ion. It is also possible that the presence of the secondary plasma re-ionizes energetic neutral species, though this is less likely because the arrival of the energetic ions is beyond the 1 ms decay period of the secondary plasma.

Lastly, scanning electron microscope analysis of the Si witness plates shown in Fig. 8 reveals that during the 145,000 shot exposure a non-conducting thin film was deposited. Although not easily observed in a static image, the forward-facing unmasked Si witness plate exhibited charging. This is qualitatively shown by an increase in brightness of the image; it was readily observed in trying to image the sample, however. This observation correlates well with the observed deposition rates witnessed by the quartz crystal microbalance. Unfortunately, XPS analysis of this sample did not reveal adequate information that varied largely from an unexposed Si sample.

In order to provide a better understanding of what non-conducting film is deposited, a set of Si witness plates was exposed off-axis (outside of the collector optics) inside of the XCEED chamber. The collector optic was kept in place, preventing line-of-sight between the witness plates and the EUV producing plasma. The resulting XPS analysis of the surface composition is shown in Fig. 9. The masked sample provides a comparative baseline reference for the measurement, and reveals that the surface composition of an unexposed sample is roughly 65% oxygen, 30% silicon, and less than 10% carbon. When exposed to the EUV plasma

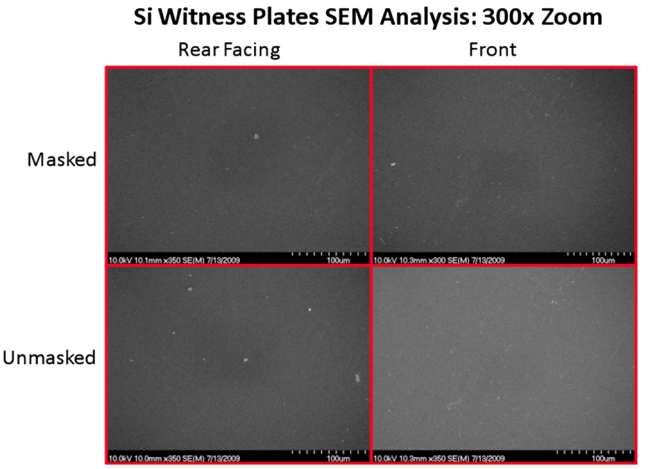

Fig. 8 The Si witness plate results show that the forward facing, unmasked sample experienced deposition of a non-conductive thin layer of either silicon oxide, tin oxide, or carbon.

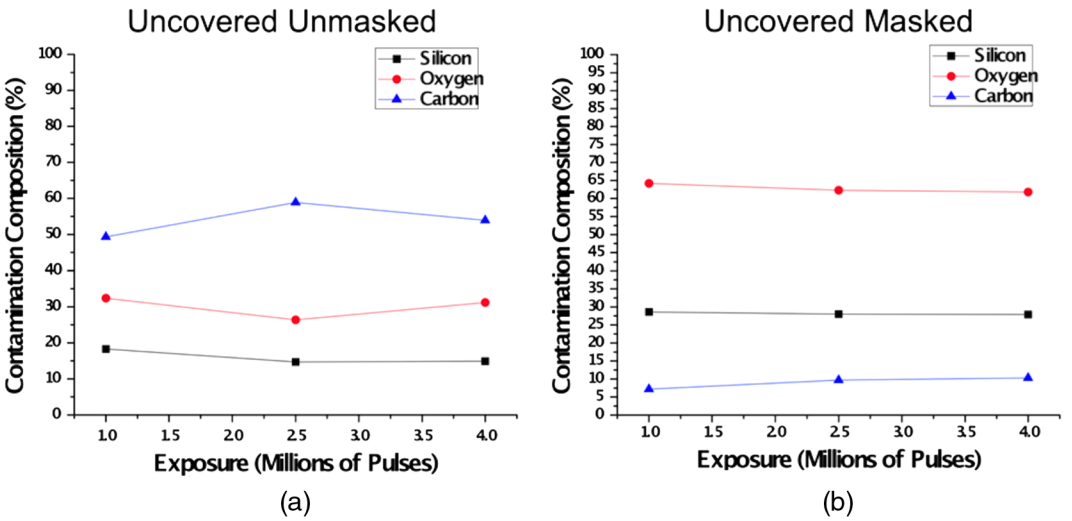

Fig. 9 Off-axis witness plates were exposed to the EUV source chamber without direct line of sight to the EUV plasma for 1, 2.5, and 4 million shots. Evident surface contamination of carbon was observed. This is due to the cracking of carbon molecules by EUV photons on the surface of the chamber.

chamber environment, however, carbon deposition occurs. EUV photons interact with carbon contamination on the walls of the chamber (originally deposited by pump oil contamination), allowing them to crack off of the surface. Further photon interaction with a surface (possible even with the collector optic in place due to the development of the secondary plasma) allows for the deposition of carbon by opening surface sites. The lack of increase in carbon composition with increasing shot count is due to a saturation of deposition as explained in Shin et al.[11]

5 Conclusion

In this investigation of the effect of debris mitigation on debris transport to the IF, it was realized that while these techniques may be functional for extending the lifetime of the collector optics, they might also have the undesired effect of transporting high-energy ions and creating induced plasmas that can cause contamination. The presence of a photoionized or electron impact excited plasma near the IF was confirmed using microchannel plates and a Faraday cup, which showed the arrival of charged flux before a direct line of sight species could arrive from the pinch. A total flux of $1.38 \pm 0.18 \times 10^{11}$ ions/cm^2 was observed with 10 mTorr and 1000 sccm, with most of this flux arriving in the first millisecond after EUV formation. A more energetic flux of ions and neutrals, originating from the EUV plasma, arrived after the dissolution of this secondary plasma with arrival times greater than 0.8 ms for the 1000 sccm, 2.25 mTorr case. The effect of these charged species was to induce deposition of a non-conducting carbon film onto the surface of whatever component faced the IF. The deposition of this film, as observed by the quartz crystal microbalance, was decreased in rate with increases of buffer gas, but was not largely affected by increases in pressure. It was also shown that using a secondary RF-plasma between the EUV source and the foil trap led to an increase in deposition rate. Maximized mitigation settings were able to reduce the deposition rate by greater than 80%. Ultimately, however, it was observed that the key component in the arrival of energetic (>100 eV) ions at the IF was the use of high Ar buffer gas flow rates of at least 1000 sccm. At these flow rates, it was seen that the arrival flux was predominately charged (>75% and as high as 97%) and removable with charged deflector plates. Using all of the mitigation techniques, except the unsuccessful secondary RF-plasma, it was shown that traditional EUV debris mitigation techniques were capable of mitigating 99.7% of the total debris reaching the IF. These techniques, however, were not capable of completely mitigating the presence of low energy ion flux throughout the exposure period, as well as the total charged and neutral high-energy flux. Although this research was performed well before the publication of these results, contractual obligations restricted presenting these results in public. Current EUV source operations reflect the results of these measurements, however, as liters of buffer gas per minute are now injected into the source, and chamber pressures are held upwards of 1 Torr.[5]

Acknowledgments

The authors would like to acknowledge the assistance of SEMATECH Inc. in funding and contributing to the development of SNIFFED. Furthermore, part of this research was carried out in the Frederick Seitz Materials Research Laboratory Central Facilities, University of Illinois, which are partially supported by the U. S. Department of Energy under Grant DEFG02-91-ER45439. Lastly, undergraduate students Daniel Organ and Piyuum Zonooz provided valuable assistance, without which this would could never have been accomplished.

References

1. M. Masnavi, "Estimation of optimum density and temperature for maximum efficiency of tin ions in z discharge extreme ultraviolet sources," *J. Appl. Phys.* **101**(3), 033306 (2007).
2. E. L. Antonsen, "Ion debris characterization from a z-pinch extreme ultraviolet light source," *J. Appl. Phys.* **99**(6), 063301 (2006).
3. K. Nishihara, "Plasma physics and radiation hydrodynamics in developing an extreme ultraviolet light source for lithography," *Phys. Plasmas* **15**(5), 056708 (2008).
4. D. N. Ruzic, "Origin of debris in EUV sources and its mitigation," in *EUV Sources for Lithography*, V. Bakshi, Ed., SPIE Press, Bellingham, WA, p. 958 (2006).

5. I. V. Fomenkov, "Laser-produced plasma light source for euvl," in *Proc. SPIE* **7636**, 763639 (2010).
6. D. N. Ruzic and S. N. Srivastava, "Normal incidence (multilayer) collector contamination," in *EUV Lithography*, V. Bakshi, Ed., SPIE Press, Bellingham, WA, p. 285 (2008).
7. M. J. Neumann, "Plasma cleaning of lithium off of collector optics material for use in extreme ultraviolet lithography applications," *J. Microlithogr. Microfabr. Microsyst.* **6**(2), 023005 (2007).
8. S. N. Srivastava, "Lifetime measurements on collector optics from Xe and Sn extreme ultraviolet sources," *J. Appl. Phys.* **102**(2), 023301 (2007).
9. E. V. Lopez, "Origins of debris and mitigation through a secondary rf plasma system for discharge-produced euv sources," *Microelectron. Eng.* **77**(2), 95–102 (2005).
10. J. Sporre, "Ionic debris measurement of three extreme ultraviolet sources," *J. Appl. Phys.* **106**(4), 043304–043304 (2009).
11. H. Shin, "Reflectivity degradation of grazing-incident euv mirrors by euv exposure and carbon contamination," *Microelectron. Eng.* **86**(1), 99–105 (2009).

Biographies and photos of the authors are not available.